View metadata, citation and similar papers at core.ac.uk
brought to you by CORE
provided by NASA Technical Reports Server

Surface characterization of carbon fiber reinforced polymers by single-shot picosecond laser induced breakdown spectroscopy

Rodolfo Ledesma [a,*], Frank Palmieri [b], John Connell [b], William Yost [b], and James Fitz-Gerald [a]

[a] Department of Electrical and Computer Engineering, University of Virginia, Charlottesville, Virginia 22904, USA
[b] NASA Langley Research Center, Hampton, Virginia 23681, USA

* Corresponding author.
E-mail address: ril2yn@virginia.edu (R. Ledesma).

Abstract

Adhesive bonding of composite materials requires reliable monitoring and detection of surface contaminants as part of a vigorous quality control process to assure robust and durable bonded structures. Surface treatment and effective monitoring, prior to bonding, is essential in order to obtain a surface which is free from contaminants that may lead to inferior bond quality. In this study, the focus is to advance the laser induced breakdown spectroscopy (LIBS) technique by using pulse energies below 100 μJ (μLIBS) for the detection of low levels of silicone contaminants in carbon fiber reinforced polymer (CFRP) composites. Various CFRP surface conditions were investigated by LIBS using ~10 ps, 355 nm laser pulses with pulse energies below 30 μJ. Time-resolved analysis was conducted to optimize the gate delay and gate width for the detection of the C I emission line at 247.9 nm to monitor the epoxy resin matrix of CFRP composites and the Si I emission line at 288.2 nm for detection of silicone contaminants in CFRP. To study the surface sensitivity to silicone contamination, CFRP surfaces were coated with polydimethylsiloxane (PDMS), the active ingredient in many mold release agents. The presence of PDMS is studied by inspecting the Si I emission lines at 251.6 nm and 288.2 nm. The measured PDMS areal densities range from 0.15 to 2 μg/cm^2. LIBS measurements were performed before and after laser surface ablation. The results demonstrate the successful detection of PDMS thin layers on CFRP using picosecond μLIBS.

Keywords: LIBS, Picosecond, Laser ablation, Surface characterization, Carbon fiber reinforced polymer

1. Introduction

In the aerospace industry, the use of carbon fiber reinforced polymers (CFRP) has enabled significant weight and fuel savings, leading to more economical and environmentally friendly (fewer emissions) large transport aircraft. To further advance aircraft performance and/or reduce manufacturing costs, there is a desire to replace mechanical fasteners with adhesive bonds [1]. Presently, for primary structures on commercial transport aircraft to meet certification criteria designated by the Federal Aviation Administration (FAA), adhesively bonded assemblies often rely on arrest features. Adhesive bonding is used in secondary aircraft structures (e.g. flight control surfaces, leading and trailing edges, and engine cowls) and has demonstrated excellent reliability [1]. In cases where failures have occurred, the cause is often traced back to improper handling of materials, and process controls. Such process controls involve surface treatment and characterization to ensure that the surface has been chemically activated and is free of contaminants.

Silicone based mold release agents are used during the fabrication of CFRP parts, and can cause surface contamination. Silicone can penetrate hundreds of nanometers into the CFRP matrix [2,3], and depending on the composite, surface treatment, adhesive and bonding process, silicone contamination can interfere with bonding even at low concentrations (0.8 μg/cm^2) [4].

Laser treatment can be used to remove contaminants from CFRP surfaces, and roughness can be created by the adequate adjustment of laser parameters, such as the laser pulse power, scan speed, and pulse frequency. By judiciously choosing the laser ablation parameters, it is possible to control the laser-CFRP interactions. In this way, superficial contaminants can be selectively removed without damaging the carbon fibers near the surface and without thermally decomposition of the CFRP matrix resin [4-7].
Effective techniques for monitoring the pre-bonding surface conditions are crucial to obtain adherent surfaces free from bond-degrading contaminants. Pre-bonding surface treatment and surface contamination detection are necessary to enhance surface conditions of aerospace composites prior to adhesive bonding and to improve the reliability of the bonded structures, so they can thus meet FAA-designed certification criteria for aircraft structures. From a practical viewpoint, the ability to detect contaminants must be sensitive, rapid, amenable to automation, and must require minimal or no sample preparation in order for it to be adopted by industry.
In this paper, laser induced breakdown spectroscopy (LIBS) is investigated for monitoring the presence of silicone contamination on CFRP materials. Microjoule picosecond laser pulses can produce high peak power levels that can surpass the optical breakdown thresholds of many materials. Picosecond pulses are shorter than the thermal relaxation times of polymers, leading to minimum heat transfer to the material outside the laser-excited volume. Most of the ultrashort pulse energy induces photochemical ablation, and consequently, there is minimal thermal stress. Low-energy pulses are required to minimize the ablation damage to the composite surface during LIBS analyses. The aim of this paper is to demonstrate that single UV picosecond pulses can be used for LIBS analysis of silicone contaminants on CFRP. The LIBS measurements were conducted with single laser shots on previously untested, i.e. “fresh”, surfaces at low pulse energies. Performing LIBS with laser pulse energies below 100 μJ (μLIBS) [8,9] can minimize surface ablation and increase surface sensitivity. In this study, CFRP surfaces were contaminated with polydimethylsiloxane (PDMS), a major constituent in silicone based mold release agents, in a controlled fashion to produce thin contamination layers. The panels contaminated with PDMS were analyzed by LIBS prior to and after laser ablation to determine the ability of the laser treatment process to remove silicone as well as the ability of LIBS to detect very low levels of silicone.

2. LIBS

LIBS is an elemental characterization technique that detects the photonic emissions from the laser induced plasma plume to obtain the chemical information of a target material. The hot induced plasma plume generated by the laser pulse expands into the ambient gas. As the plasma plume cools down, it emits photons at different wavelengths that are characteristic to the target material. Some advantages of LIBS are that measurements can be performed rapidly and without sample preparation. LIBS can provide chemical analysis of elements in different forms (solid, liquid, or gaseous).

2.1 Laser-material interactions

For picosecond and ultrashort pulses, the primary interaction is plasma-matter, which affects the electrons in the solid. The electrons are heated by the laser pulse, and the transfer of energy to the lattice by collisions takes more time than the incident laser pulse duration. Picosecond and ultrashort pulses excite the target surface rapidly. For polymers, if the laser energy irradiated on the material is sufficient, bond dissociation occurs by multiphoton transition. Such a photochemical mechanism produces mechanical stress to break bonds, and the material is removed from the target surface by fragmentation [10,11]. There is minimal energy transferred to the regions outside the irradiated material volume, producing less thermal-stress in the material.

2.2 Plasma emission processes

The laser radiation interacts with the electrons in the material, causing ionization. The high-temperature dense plasma expands at supersonic velocities into the ambient gas [12]. During early stages of the plasma plume, free electrons, atoms, and ions collide and interact. At this time, the plasma emission is governed by continuum radiation caused by free-free transitions, or Bremsstrahlung [13], along with free-bound transitions, or radiative recombination [14]. In Bremsstrahlung, a free electron loses kinetic energy and emits photons at different wavelengths, and the electron remains free after emitting photons. In the recombination process, a free electron is completely stopped by the electromagnetic field of an ion. The free electron is then captured by the ion, and the excess of kinetic energy is released as photons, producing recombination radiation. Bremsstrahlung and recombination radiation are responsible for continuum emission.
As the plasma plume expands and cools down, bound electrons in atoms and ions descend through the quantized energy states, producing characteristic emission lines that are element specific. This process is called bound-bound transition and is responsible for the optical emission lines. In this process, the emitted photon that corresponds to the transition from state k to state i has a wavelength λ_{ki} and frequency ν_{ki} as follows,

$$\lambda_{ki} = \frac{hc}{E_k - E_i} = \frac{c}{\nu_{ki}} \qquad (1)$$

Where h is Planck's constant, c the speed of light, and E_k and E_i the energies of the upper and lower state.

2.3 μLIBS

The extension of LIBS toward lower pulse energies, typically < 100 μJ, is known as μLIBS [15-18]. The benefits of μLIBS include the use of the lower energy pulses and higher pulse frequencies that most modern laser systems yield. In μLIBS, the decay time of the emission line couples with an even faster decay of the continuum emission, making possible the detection of the LIBS signal using ungated detectors [15-17]. The improved ratio of line-to-continuum emission and small pulse energy in μLIBS can be optimized to achieve the limit of detection (LOD) using conventional LIBS, which is in the mJ regime [18]. In addition, the ablation crater size decreases with lower pulse energies, and thus, the technique may be considered nondestructive. Also, since the ablation crater dimensions are reduced, the spatial (lateral) and depth resolutions are enhanced [8,19]. Moreover, given the lower laser pulse energies, compact and economic laser sources can be employed in LIBS systems.

3. Experimental

3.1 Materials

Unidirectional CFRP panels (30.5 cm x 30.5 cm) were fabricated from eight plies of unidirectional Torayca P2302-19 (T800H/3900-2) prepreg. The curing process was performed in an autoclave at 177 °C and 690 kPa. Release from the caul plate was achieved using Airtech A4000V release film, a fluorinated ethylene propylene (FEP) film, which was placed between the caul plate and the prepreg plies. For LIBS measurements, the laminates were cut with a water jet into square samples of 1.27 cm x 1.27 cm.
X-ray photoelectron spectroscopy (XPS) was performed on a Surface Science Instruments SSX-100 spectrometer with a monochromatic Al K-alpha X-ray (1.486 keV photon energy) source. The spot size was 800 μm x 800 μm.

3.2 Sample contamination

Contamination on CFRP samples was produced by spraying PDMS diluted with hexanes to various concentrations, leading to different layer thicknesses. The PDMS coated samples were dried at 100 °C for 1 hour. Using witness p-type Si[100] wafers, PDMS thicknesses were measured by using variable angle spectroscopic ellipsometry (VASE) using a J.A. Woollam VB-400 control module and HS-190 scanning monochromator. Data were collected in the wavelength range from 370 nm to 900 nm with a 10 nm step size at three incident angles: 65°, 70°, and 75°. From these measurements, the thickness of PDMS on the CFRP surfaces was inferred.

3.3 Laser ablation

Laser ablation was performed with a Nd:YVO_4 laser system (Atlantic 20-355, EKSPLA) operated at 355 nm with a nominal pulse duration of ~10 ps, 80 mW average power, and 400 kHz pulse frequency. The calculated average photon flux of the focused laser beam was 7.17 x 10^{22} photons/s/cm^2. The average laser power was measured with a thermopile sensor (30A-BB-18, Ophir-Spiricon) and a laser power meter (Nova II, Ophir-Spiricon). During ablation, the CFRP sample was held stationary while the galvanometer unit scanned the composite surface. CFRP specimens were laser ablated with parallel lines, which were produced in the fiber orientation at 12.7 μm line pitch and 25.4 cm/s scan speed.

3.4 Surface morphology

Depth measurements of LIBS craters produced with single shots were performed with an optical surface profiler (NewView 6000, Zygo) equipped with a 20X Mirau objective and a 1X zoom lens. CFRP surfaces were coated with Pd-Au for surface morphology analysis using a JEOL JSM-5600 scanning electron microscope (SEM) operated at an accelerating voltage of 15 kV.

3.5 LIBS

The schematic diagram of the LIBS system is shown in Fig. 1. The Nd:YVO_4 (Atlantic 20-355, EKSPLA) laser was operated at 355 nm with a nominal pulse duration of ~10 ps. The laser beam was focused by an f-theta lens (S4LFT6062/075, Sill Optics) for a wavelength of 355 nm and with an effective focal length of 250 mm. The LIBS emission was measured using a 328 mm, f/4.6 Schmidt-Czerny-Turner (SCT) spectrograph (IsoPlane SCT 320, Princeton Instruments). The spectral response was recorded using an electron-multiplier intensified charge-coupled device (emICCD) camera (PI-MAX4: 1024 EMB, Princeton Instruments). The plasma emission was collected with a collimator and guided to the spectrograph via an optical cable with 19, 200-μm fibers. A grating with 1200 grooves/mm, blazed at 300 nm, was used for all the experiments. The slit width was kept at 10 μm. The emICCD camera was externally triggered by the laser trigger output.

The LIBS spectra were generated by averaging 15 frames of 10 single laser shots. The target surface was moved with the XY stage after each single shot to expose a fresh surface for each incident pulse. The 10 single laser shots were accumulated on the CCD sensor.

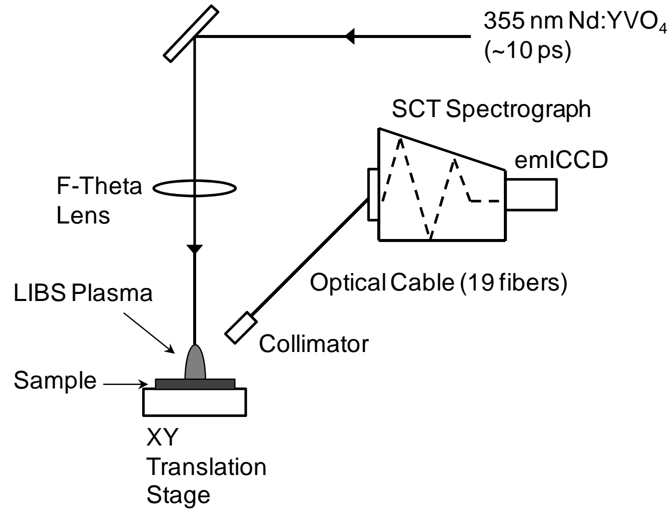

Figure 1. Schematic diagram of the LIBS system for the detection of contaminants on CFRP.

4. Results and discussion

4.1 Surface morphology

The ablation threshold for ablation depth per pulse is calculated by single-shot ablated craters with [20],

$$d = \delta \ln\left(\frac{E_p}{E_{th}}\right) \qquad (1)$$

where d is the single-shot ablation depth, δ the effective optical penetration depth, E_p the laser pulse energy, and E_{th} the threshold energy for laser ablation.

Figure 2 shows the linear relationship between the single-shot ablation depth and the logarithm of the laser pulse energy. The error bars indicate 1σ standard deviation. The slope of the logarithmic fit in Eq. (1) yields $\delta = 0.33 \pm 0.07$ µm. The single laser shots ablated only the top layer of epoxy resin without interacting with the carbon fibers. Therefore, the threshold energy of the matrix epoxy resin calculated for a laser pulse duration of ~10 ps focused on CFRP is 2.4 µJ.

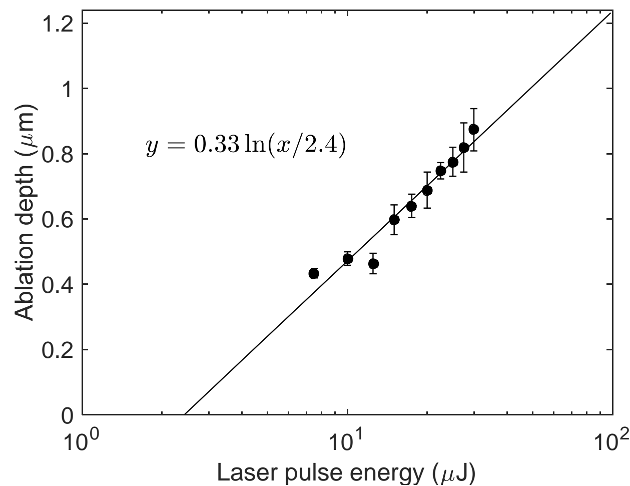

Figure 2. Single-shot ablation depth measurements of CFRP. The solid line represents the logarithmic fit according to Eq. (1), which yields an effective optical penetration depth of $\delta = 0.33 \pm 0.07$ µm and an ablation threshold of $E_{th} = 2.4$ µJ.

Figure 3 shows the SEM images of the craters produced on CFRP using single laser shots. The craters show no melted or redeposited material around the craters. As the pulse energy increases above 15 µJ, an inner crater starts forming due to the increasing energy absorption of the material in the same direction of the laser beam. In addition, the crater deepens faster than it widens. In contrast to the crater contour, the inner crater has a circular shape. Similar to the external major crater, the inner crater does not exhibit melted or redeposited material around its contour. In all the single-shot LIBS measurements, the pulses do not interact with the carbon fibers underneath the top epoxy resin layer, as shown in the SEM images.

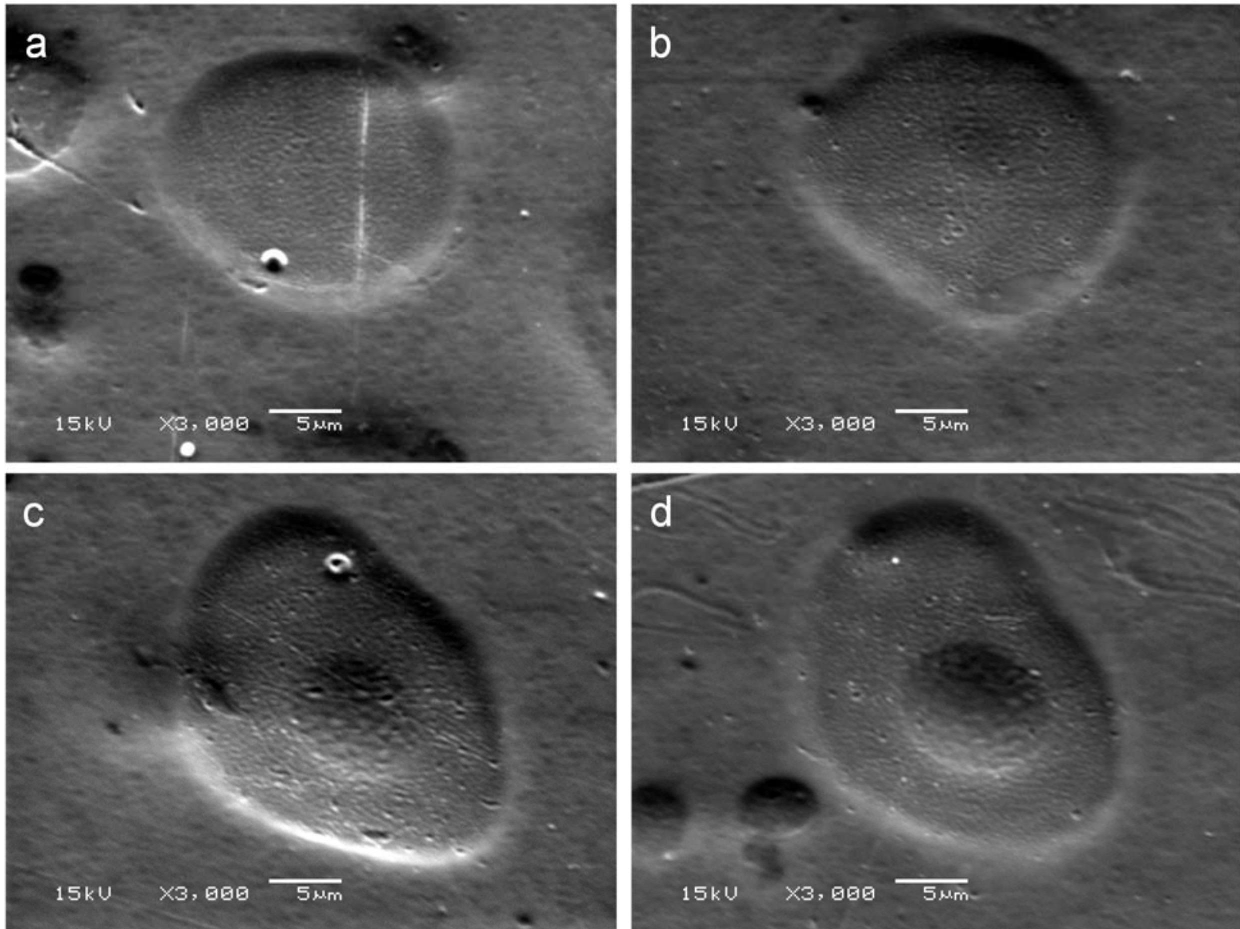

Figure 3. SEM images of ablated craters on CFRP using single picosecond pulses of a) 7.5 µJ (3.77 J/cm^2), b) 15 µJ (7.53 J/cm^2), c) 25 µJ (12.55 J/cm^2), and d) 30 µJ (15.06 J/cm^2).

4.2 Signal-to-noise ratio analysis

The signal-to-noise ratio (SNR) is a quantitative measure that defines the relative intensity between the LIBS signal and the noise. The SNR is calculated as,

$$SNR = \frac{I_p}{3\sigma_b} \qquad (2)$$

where I_p is the background-corrected height of the peak of interest, and σ_b is the standard deviation of a background-corrected spectrally quiet region away from the peak. The noise level is three times σ_b. The limit of detection (LOD) occurs when SNR = 1.

The emission characteristics of the elements and the matrix composition will affect the SNR of an emission line. An untreated, unintentionally contaminated CFRP was tested for the detection of the C I emission line and the Si I emission line. The C I emission at 247.9 nm corresponds to the transition $2s^2 2p3s\ ^1P^o \rightarrow 2s^2 2p^2\ ^1S$, and the Si I emission line at 288.2 nm to $3s^2 3p4s\ ^1P^o \rightarrow 3s^2 3p^2\ ^1D$. The C I emission line is used to monitor the epoxy resin matrix from the CFRP sample, while the Si I emission line allows the monitoring of the silicone that may be present from the CFRP manufacturing. Silicone is the main component for many mold release agents used in composite fabrication. The LIBS spectra were acquired with a gate delay of 5 ns and a gate width of 250 ns. The gate width was chosen to collect all the plasma emission and to minimize noise integration on the CCD sensor. The dark noise was removed in the final frame. The spectral baseline, caused by the continuum emission, was corrected prior to calculating the SNR. Figure 4 shows the SNR for the C I emission line at 247.9 nm and the Si I emission line at 288.2 nm for different laser pulse energies. Each SNR data point is an average of three SNR measurements, and the error bars indicate 1σ standard deviation. The SNR for the C I emission at 247.9 nm increases at a faster rate than that of the Si I emission at 288.2 nm. The reason is that more ablated material forms the plasma, and thus, there is an increase in C concentration that will contribute to the plasma emission. However, the concentration of Si does not significantly increase with the laser pulse energy. This may signify that the silicon compounds are localized to a uniform layer near the surface. It has been demonstrated that ablated material close to the surface contributes more to the plasma emission [19,21]. This is also explained by the fact that the number of atoms ejected in an excited state represents a small fraction of the atoms ejected as neutrals, clusters, liquid droplets, or solid fragments [21]. Therefore, the number of emitted photons is smaller than the number of atoms ablated from the target material.

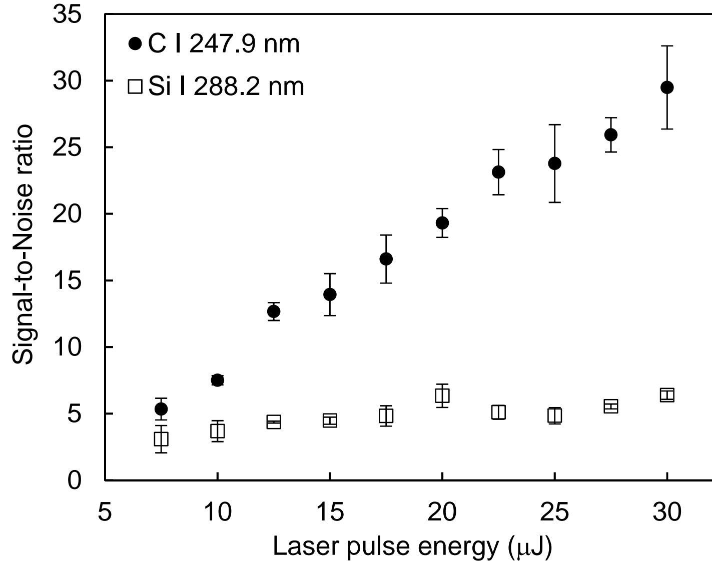

Figure 4. Evolution of SNR of the C I emission line at 247.9 nm and the Si I emission line at 288.2 nm for different laser pulse energies. The gate delay and gate width were set to 5 ns and 250 ns, respectively.

4.3 Time-resolved analysis

The SNR varies for different gate delays and laser pulse energies. The plasma plume characteristics influence the optimum gate delay required to maximize the SNR. An untreated, unintentionally contaminated CFRP was tested to examine the SNR of C I at 247.9 nm and Si I at 288.2 nm as a function of the gate delay. A gate width of 200 ns was used in order to collect the plasma emissions and minimize noise accumulation on the CCD sensor. Figure 5 shows the SNR for the C I emission line at 247.9 nm for 15 μJ and 30 μJ pulse energy as a function of the gate delay. Each SNR data point is an average of three SNR measurements, and the error bars indicate 1σ standard deviation. Figure 6 shows the SNR for the Si I emission line at 288.2 nm for 15 μJ and 30 μJ laser pulse energy. For both laser energies, the optimum gate delays are similar for the C I and Si I emission lines from the CFRP surface. The optimum gate delay increases with the laser pulse energy. As the pulse energy increases, the plasma volume consists of more ablated material. For higher pulse energies, the plasma plume will take longer to expand and reach its optimum temperature and density for emission lines. For lower pulse energies, the generated plasma plume is smaller and less dense, and therefore the continuum emission and temperature decay faster.

A pulse energy of 15 μJ was selected for surface characterization in order to increase the surface sensitivity of the LIBS measurements using single shots and to minimize the ablation damage. This will allow the detection of surface contamination without disturbing the bulk or the carbon fibers underneath the top epoxy resin layer. In addition, with the chosen pulse energy, the quality was not significantly compromised, assuring the correct spectral analysis for chemical identification.

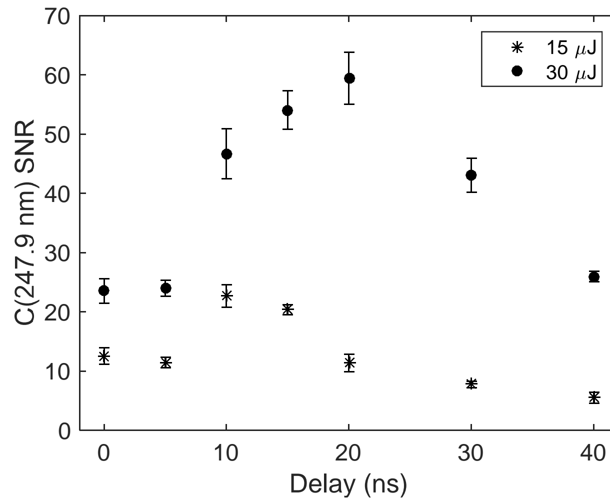

Figure 5. Variation of SNR as a function of the gate delay for the C I (247.9 nm) emission line for laser pulse energies of 15 μJ and 30 μJ. The sample was an untreated, unintentionally contaminated CFRP.

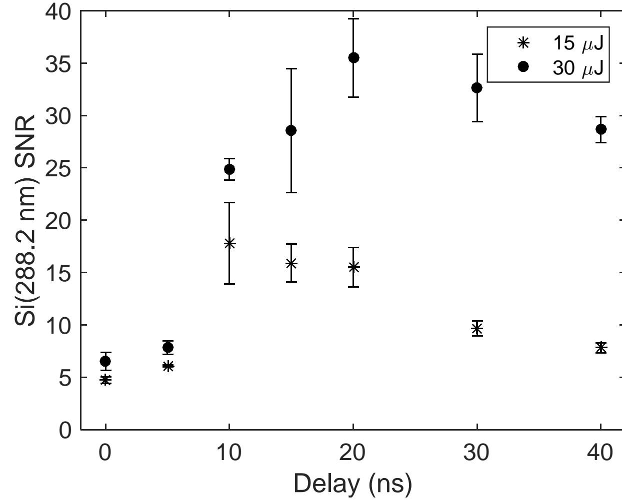

Figure 6. Variation of SNR as a function of the gate delay for the Si I (288.2 nm) emission line for laser pulse energies of 15 µJ and 30 µJ. The sample was an untreated, unintentionally contaminated CFRP.

Figure 7 shows the spectra of an untreated, unintentionally contaminated CFRP surface for different gate delays. The spectral range is 240 nm to 260 nm. To improve the SNR, each spectrum was obtained by averaging 15 frames of 10 single laser shots, and each single shot was on a fresh surface. Within that wavelength range, the main emission lines are C I at 247.9 nm and Si I at 251.6 nm. The dark noise was subtracted by online correction, but the background from the continuum emission was not corrected. Increases in the gate delay reduced the contribution of the continuum emission to the spectrum, allowing the emission lines to be more defined. For the C I emission at 247.9 nm, the optimum delay was 10 ns for a laser pulse energy of 15 µJ, as shown in Fig. 5. The spectra (figure 8) shows an untreated, unintentionally contaminated CFRP surface for different gate delays. The spectral range was 278 nm to 294 nm. The spectral range was selected to inspect the Si I emission line at 288.2 nm. For the Si I emission at 288.2 nm, the optimum delay was 10 ns for a laser pulse energy of 15 µJ, as also shown in Fig. 6. Therefore, for both the C I (237.9 nm) and Si I (288.2 nm) emission lines, the optimum delay is 10 ns for a pulse energy of 15 µJ. The C I emission line at 247.9 nm indicates the detection of the epoxy resin matrix of the CFRP sample. The Si I emission lines at 251.6 nm and 288.2 nm reveal the presence of silicon compounds. The use of silicone based mold release agents are a source of silicon compounds that may have diffused in the epoxy CFRP bulk matrix during fabrication. The Si I emission lines are of interest in order to detect silicone based contaminants that interfere with adhesive bonding even at low concentrations [4].

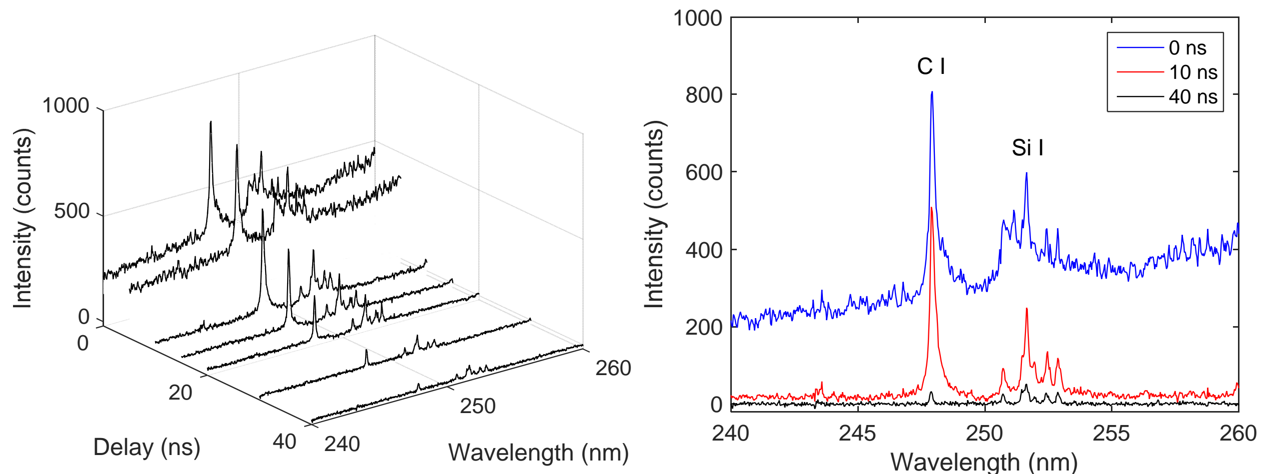

Figure 7. Dark noise corrected spectra from an untreated CFRP using 15 μJ pulses for different gate delays. The main emission lines are C I at 247.9 nm and Si I at 251.6 nm. Each spectrum was obtained by averaging 15 frames of 10 single laser shots. Each single shot was on a fresh surface. The continuum emission decreases as the gate delay increases, allowing more defined emission lines.

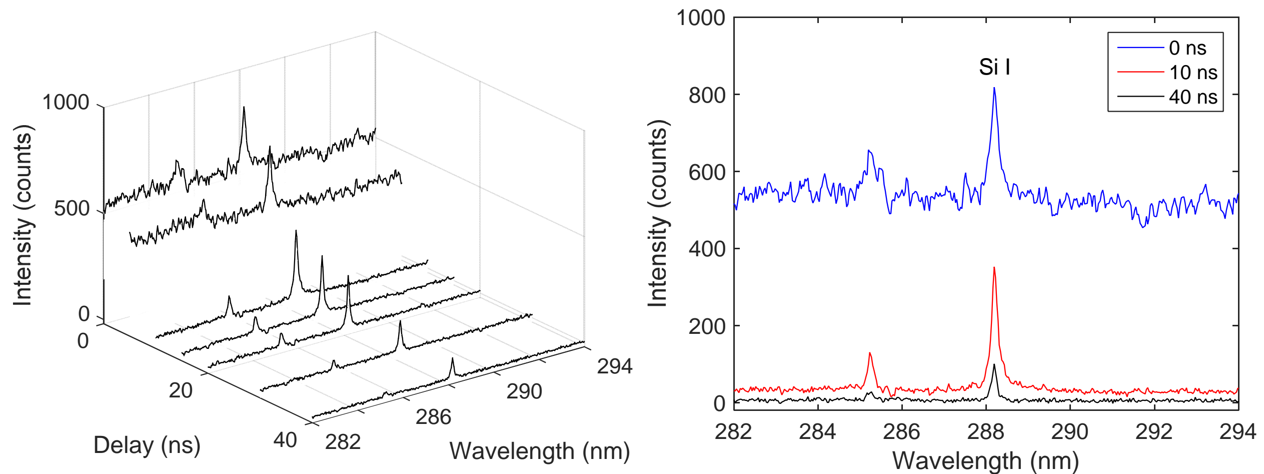

Figure 8. Dark noise corrected spectra from an untreated CFRP using 15 μJ pulses for different gate delays. The main emission line is Si I at 288.2 nm. Each spectrum was obtained by averaging 15 frames of 10 single laser shots. Each single shot was on a fresh surface. The continuum emission decreases as the gate delay increases, allowing more defined emission lines.

4.4 Laser surface ablation

Laser ablation for surface contamination removal and surface preparation, prior to adhesive bonding, was employed for both laser surface treatment and LIBS characterization. This allows for rapid feedback from LIBS concerning surface condition.
CFRP samples were inspected using LIBS to detect PDMS prior to and after laser surface ablation. Prior to PDMS contamination, the CFRP surfaces were degreased with a mild soap solution, rinsed thoroughly with water, and then dried. The control sample was not coated with PDMS and served as a reference surface. Table 1 shows the characteristics of the PDMS coatings. The PDMS areal number density n was calculated by

$$n = \frac{\rho N_A l}{M} \qquad (3)$$

where ρ is the density of PDMS, N_A Avogadro's number, l the PDMS film thickness, and M the PDMS molecular weight. The PDMS film thickness is determined by ellipsometry on smooth p-type Si[100] surfaces. The PDMS distribution on Si substrates will differ from the thickness of PDMS distributed on CFRP surfaces due to their roughness and heterogeneity.

Table 1. Characteristics of the PDMS coatings on CFRP surfaces. The PDMS thickness was characterized by ellipsometry. The PDMS areal density and areal number density were calculated. The latter was determined using Eq. (3). The mean values are indicated along with their 1σ standard deviations.

Thickness	Areal density	Areal number density

(nm)	(μg/cm^2)	(10^{12} molecules/cm^2)
0 (Control)	0	0
1.54 ± 0.08	0.15 ± 0.008	2.5 ± 0.13
2.12 ± 0.03	0.2 ± 0.003	3.5 ± 0.05
2.63 ± 0.09	0.25 ± 0.009	4.3 ± 0.15
2.73 ± 0.1	0.26 ± 0.01	4.5 ± 0.15
3.56 ± 0.62	0.34 ± 0.06	5.8 ± 1
20.49 ± 0.03	2 ± 0.003	33.6 ± 0.05

Figure 9 shows the LIBS spectra obtained from select CFRP surface conditions prior to laser ablation. The select PDMS areal densities were 0.15 μg/cm^2, 0.26 μg/cm^2, 0.34 μg/cm^2, and 2 μg/cm^2. The emission lines of interest are C I at 247.9 nm and Si I at 288.2 nm. Other neutral Si lines are detected between 250 nm and 255 nm, the strongest peak being at 251.6 nm. The surfaces with higher PDMS areal density show stronger emission intensities for the neutral Si species between 250 nm and 255 nm. The intensity of the neutral C peak at 247.9 nm remains similar for all surface conditions. The intensity of the Si emission line at 288.2 nm for the control sample differs significantly from the PDMS coated surfaces.

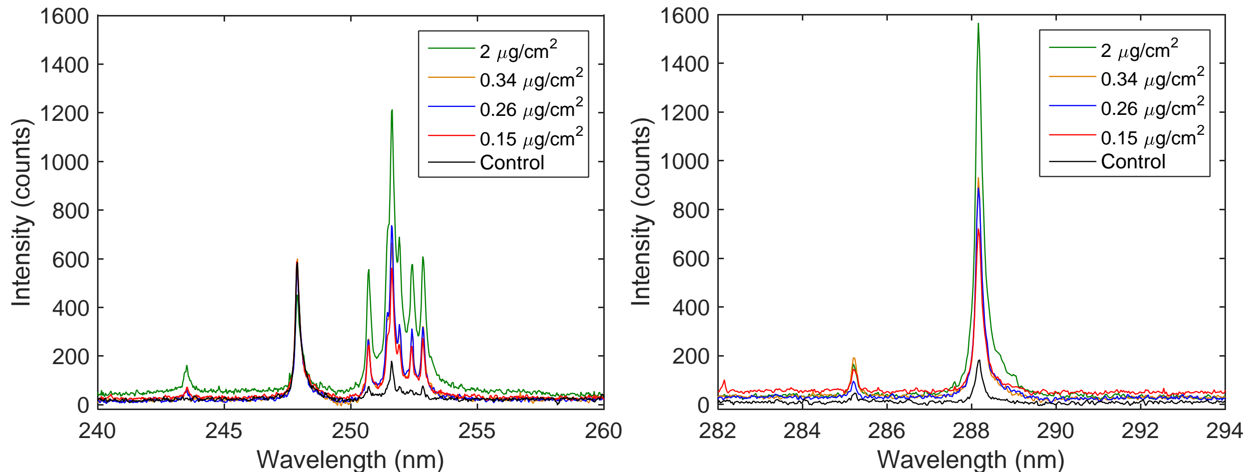

Figure 9. LIBS spectra prior to laser ablation for the UV regions from 240 nm to 260 nm and from 282 nm to 294 nm. The peaks of interests are 247.9 nm for C I and 251.6 nm and 288.2 nm for Si I. Other neutral Si lines are detected between 250 nm and 255 nm.

The CFRP surfaces were laser ablated with an energy fluence of 0.1 J/cm^2, a scan speed of 25.4 cm/s, and a line pitch of 12.7 μm. Figure 10 shows the laser ablated surface of the control CFRP sample. The parallel lines were laser ablated in the fiber direction, as shown in the SEM images in Fig. 10. The ablated lines produced a surface pattern without disturbing the carbon fibers underneath the top layer of epoxy resin. As shown in Fig. 10(b), the laser ablated portion of the surface (left) is rougher than the untreated surface (right).

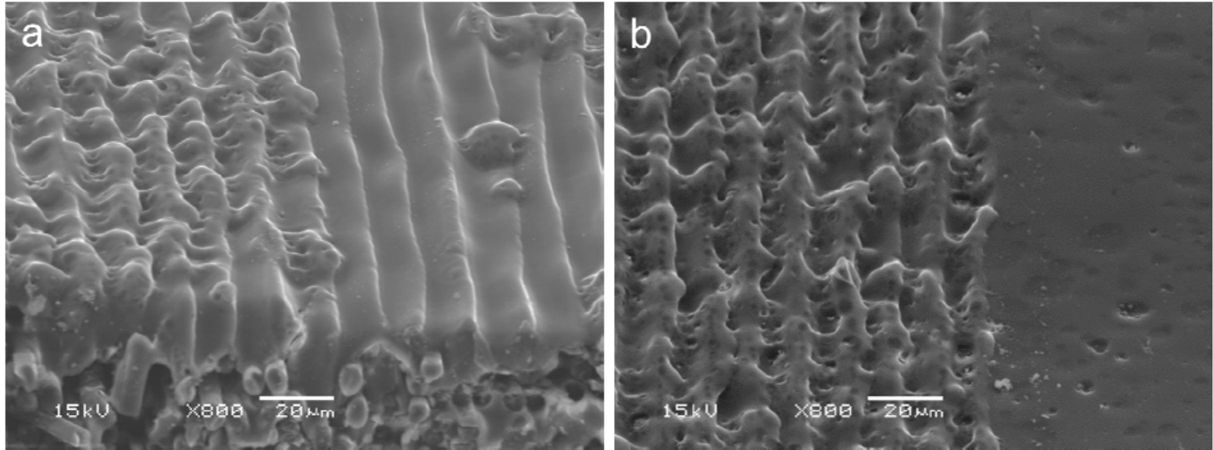

Figure 10. SEM images of the control CFRP surface after laser ablation. (a) The parallel lines were ablated in the fiber direction with a line pitch of 12.7 μm. (b) This SEM image shows the morphology differences between a laser ablated surface and an untreated region.

After laser ablation, the CFRP surfaces were characterized with LIBS. Figure 11 shows the spectra of the different CFRP surface conditions after laser ablation. In contrast to Fig. 9, the neutral Si lines between 250 nm to 255 nm decrease significantly following laser ablation. For the control surface, the Si I peak at 251.6 nm cannot be detected and is negligible in intensity. For the PDMS contaminated surfaces, there is still Si detected indicating that silicone remains present on the surface. For the wavelength range between 282 nm and 294 nm, the Si I emission line at 288.2 nm decreases significantly in comparison to that of Fig. 9. The detection of Si peaks after laser ablation means that the silicone contaminant was not removed completely from the CFRP surfaces under these ablation conditions.

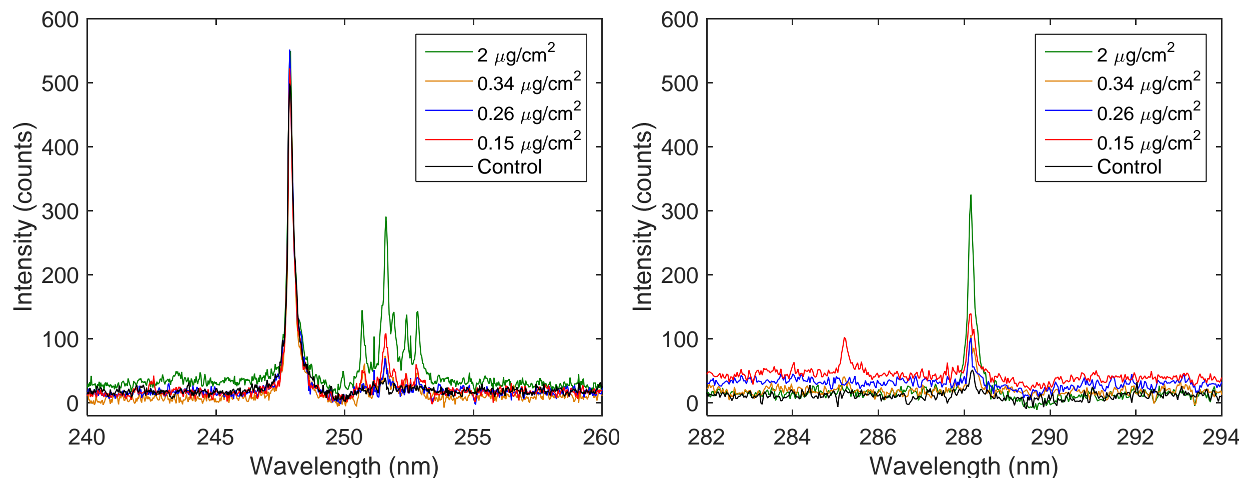

Figure 11. LIBS spectra after laser ablation for the UV regions from 240 nm to 260 nm and from 282 nm to 294 nm. The peaks of interests are 247.9 nm for C I and 251.6 nm and 288.2 nm for Si I. Other neutral Si lines are detected between 250 nm and 255 nm.

The data are presented as the ratio of the Si and C peak heights before and after laser ablation as shown in Fig. 12. The Si/C peak ratio was used as an analytical parameter to compare the relative abundance of Si from silicone and C from the matrix resin. The bars represent the mean values and the error bars indicate 1σ standard deviation. The selected peaks for Si I are 251.6 nm and 288.2 nm. The level of silicone contaminant was significantly reduced after laser ablation. For the control sample, the ratio Si/C for Si

(251.6 nm) decays from 0.27 to 0.042, while for Si (288.2 nm) the ratio decreases from 0.3 to 0.063. Considering the surface with the highest PDMS areal density (2 μg/cm^2), the Si/C ratio decays from 2.78 to 0.51 from Si I at 251.6 nm and from 3.91 to 0.64 for Si I at 288.2 nm. The sensitivity of the LIBS system was able to readily detect the low levels of silicone contamination (3.4 ± 0.2 at.% using the Si 2p peak measured by XPS before laser ablation) on the control sample. Thus, LIBS can detect silicone contaminants at concentrations less than those known to pose a threat to adhesive bonding with this CFRP material system (0.8 μg/cm^2) [4], requires no sample preparation, and can provide rapid feedback of Si contamination levels. With the Si/C peak ratio as an analytical metric, it is possible to differentiate the control surface from the contaminated surfaces, as well as the laser treated surfaces from the untreated ones.

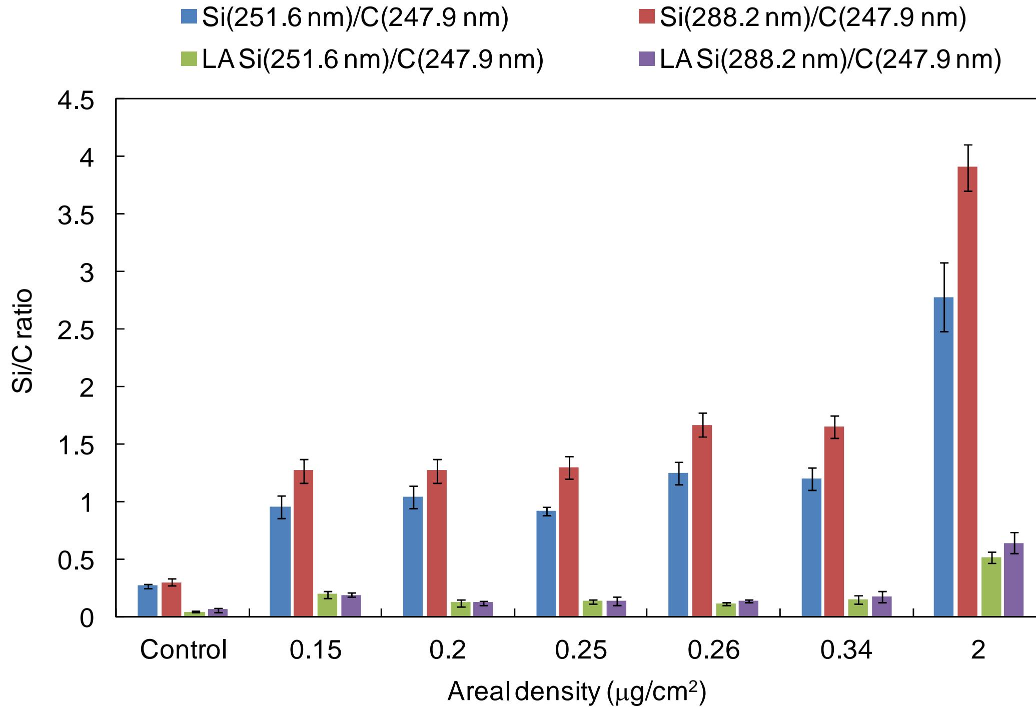

Figure 12. Si/C ratios for CFRP samples before and after picosecond laser ablation (LA). All the surfaces, except for the control, were coated with PDMS at different concentrations, producing different PDMS areal densities.

Conclusions

In this study, picosecond μLIBS was investigated for detection of silicone contaminants on CFRP surfaces. Using single laser shots, the ablation threshold of the top layer of epoxy resin in the CFRP material system was found to be 2.4 μJ. From the ablation depth analysis, the effective optical penetration depth was determined to be 0.33 ± 0.07 μm. By analyzing the ablation depth for different pulse energies, it was possible to select the parameters for LIBS analysis that minimize the ablation damage and increase the sensitivity of detection of surface contaminants. The outcome from the SNR analysis showed that the silicone present in the epoxy resin matrix is localized to a uniform layer near the surface. The time-resolved analysis was applied to obtain the optimum gate delay for the collection of plasma emissions. Detection of PDMS was demonstrated using 355 nm, 15 μJ pulses. The presence of PDMS on the epoxy matrix composites increased the Si emission intensity while suppressing the C line emission from the matrix material. After laser ablation, the C line emission increased whereas the Si line emission decreased. This demonstrated that the amount of PDMS was significantly decreased after laser surface ablation. This was

corroborated by the decrease of the Si/C ratios for all the inspected CFRP surfaces. LIBS provided a rapid surface characterization before and after laser surface ablation. Each level of PDMS contamination on the CFRP surface yielded a unique spectral response that allowed the differentiation of Si levels from that of a control CFRP. The spectral response of each contaminated surface demonstrates that materials close to the surface will contribute more to the LIBS signal. Therefore, it is possible to detect low levels of silicone for different surface conditions.

Picosecond μLIBS provides sensitive detection of low levels of silicone contaminants prior to adhesive bonding of CFRP structures. By using the same laser system for both surface treatment and LIBS analysis, LIBS has potential as an in-situ technique that can be automated and integrated into the laser surface ablation process.

Acknowledgements

The authors acknowledge funding from the NASA Advanced Composites Project and thank the following personnel from NASA Langley Research Center: John Hopkins for conducting the laser ablation surface treatment, Hoa Luong and Sean Britton for laminate fabrication, and Michael Oliver for sample preparation.

References

1. R. Bossi, M. Piehl, Bonding primary aircraft structure: The issues, Manuf. Eng. 146 (3) (2011) 101-109.
2. B. Ehrhart, B. Valeske, R. Ecault, M. Boustie, L. Berthe, C. Bockenheimer, Extended NDT for the quality assessment of adhesive bonded CFRP structures, Smart Materials, Structures & NDT in Aerospace Conf., 2011.
3. P.H. Malinowski, M. Sawczaka, T. Wandowskia, W.M. Ostachowicz, A. Cenian, Characterisation of CFRP surface contamination by laser induced fluorescence, in: Proc. SPIE, Health Monitoring of Structural and Biological Systems, Vol. 9064, 2014.
4. F. Palmieri, R. Ledesma, D. Cataldo, Y. Li, C. Wohl, M. Gupta, J. Connell, Controlled contamination of epoxy composites with PDMS and removal by laser ablation, SAMPE Long Beach, 2016.
5. Y.-F. Lu, Y. Aoyagi, M. Takai, S. Namba, Laser surface cleaning in air: Mechanisms and applications, Jpn. J. Appl. Phys. 33 (1994) 7138-7143.
6. Y.-F. Lu, M. Takai, T. Shiokawa, Y. Aoyagi, Excimer-laser removal of SiO_2 patterns from GaAs substrates, Jpn. J. Appl. Phys. 33 (1994) L324-L327.
7. F. Palmieri, M. Belcher, C. Wohl, K. Blohowiak, J. Connell, Laser ablation surface preparation for adhesive bonding of carbon fiber reinforced epoxy composites, Int. J. Adhes. Adhes. 68 (2016) 95-101.
8. M.T. Taschuk, Y.Y. Tsui, R. Fedosejevs, Detection and mapping of latent fingerprints by laser-induced breakdown spectroscopy, Appl. Spectrosc. 60 (2006) 1322-1327.
9. Y. Godwal, M.T. Taschuk, S.L. Lui, Y.Y. Tsui, R. Fedosejevs, Development of laser-induced breakdown spectroscopy for microanalysis applications, Laser Part. Beams 26 (2008) 95-103.
10. M. Gedvilas, G. Raciukaitis, Investigation of UV picosecond laser ablation of polymers, in: Proc. SPIE, Workshop on Laser Applications in Europe, Vol. 6157, 2005.
11. W. Lei, Temporal and spatial characteristics of laser-induced plasma on organic materials and quantitative analysis of the contained inorganic elements, Ph.D. thesis, Université Claude Bernard Lyon 1 and East China Normal University (2012).
12. B.J. Garrison, R. Srinivasan, Laser ablation of organic polymers: Microscopic models for photochemical and thermal processes, J. Appl. Phys. 57 (1985) 2909-2914.
13. J.F. Kephart, R.P. Godwin, G.H. McCall, Bremsstrahlung emission from laser-produced plasmas, Appl. Phys. Lett. 25 (1974) 108-109.
14. G. Bekefi, C. Deutsch, B. Yaakobi, Spectroscopic diagnostics of laser plasmas, in: G. Bekefi (Ed.), Principles of Laser Plasmas, Wiley Interscience, New York, 1976, pp. 549-669.

15. M. Hidalgo, F. Martin, J.J. Laserna, Laser-induced breakdown spectrometry of titanium dioxide antireflection coatings in photovoltaic cells, Anal. Chem. 68 (1996) 1095-1100.
16. G.W. Rieger, M. Taschuk, Y.Y. Tsui, R. Fedosejevs, Comparative study of laser-induced plasma emission from microjoule picosecond and nanosecond KrF-laser pulses, Spectrochim. Acta, Part B 58 (2003) 497-510.
17. I.B. Gornushkin, K. Amponsah-Manager, B.W. Smith, N. Omenetto, J.D. Winefordner, Microchip laser-induced breakdown spectroscopy: A preliminary feasibility investigation, Appl. Spectrosc. 71 (2004) 762-769.
18. G.W. Rieger, M. Taschuk, Y.Y. Tsui, R. Fedosejevs, Laser-induced breakdown spectroscopy for microanalysis using submillijoule UV laser pulses, Appl. Spectrosc. 56 (2002) 689-698.
19. S.P. Banerjee, R. Fedosejevs, Single shot depth sensitivity using femtosecond laser induced breakdown spectroscopy, Spectrochim. Acta, Part B 92 (2014) 34-41.
20. A. Ben-Yakar, R.L. Byer, Femtosecond laser ablation properties of borosilicate glass, J. Appl. Phys. 96 (2004) 5316-5323.
21. M.T. Taschuk, Quantification of laser-induced breakdown spectroscopy at low energies, Ph.D. thesis, University of Alberta, Canada (2007).